Coupled Analysis of Electromagnetic Vibration Energy Harvester with Nonlinear Oscillation

Takahiro Sato[1], Kota Watanabe[2], and Hajime Igarashi[1], *Member, IEEE*

[1] Graduate school of Information science and technology, Hokkaido University,
Kita 14, Nishi 9, Kita-ku, Sapporo, 060-0814, JAPAN
[2] Muroran Institute of Technology

This paper presents a coupled analysis of electromagnetic vibration energy harvester (VEH) based on the nonconforming voxel FEM. In the present analysis method, the motion, Maxewell, and circuit equations are alternatively solved using the staggered method. The FE models can be generated in the present method with low computational costs. Using the coupled analysis method, the characteristics of a VEH model, which contains the magnetic material in the coil, is analyzed changing the geometric parameters. It is shown from the analysis results that the VEH model has chaotic and linear oscillations. It is also found that output power can be generated for a wide frequency range in the chaotic mode, and in the linear mode, large output power is obtained at the resonance.

***Index Terms*— Coupled problem, electromagnetic induction, energy harvesting.**

I. Introduction

The electromagnetic vibration energy harvesters (VEHs), which transform vibration to electrical energy through magnetic induction [1]-[4], have attracted attention for new small and maintenance-free power source. Using VEH, it is possible to realize wireless network systems which are free from battery replacement [5]. In order to develop practical VEH systems, the output power and bandwidth of VEH devices must be improved. To improve the output, one should design the flux path to increase the magnetic flux across the coil. The use of magnetic materials is effective to form the flux path. When using the magnetic material, the strong magnetic force acts on the oscillator. The strong magnetic force gives rise to nonlinearity in the VEH devices. It has been shown that the bandwidth can be expanded by the nonlinear oscillations [6], [7]. However, owing to complicated motion in the VEH devices under strong magnetic force, the output power cannot be accurately evaluated based on a simple spring-damper model [8]. To accurately analyze the behavior and output of such devices, the coupling of motion, electromagnetic field, and electrical circuit must be considered.

In this paper, a new coupled analysis method for VEH devices will be introduced, in which Maxwell, motion, and circuit equations are solved alternatively using the staggered method [9]. Moreover, the electromagnetic field is analyzed using the nonconforming voxel FEM (voxel-FEM) [10] in which one can generate the FE models for any device shapes with low computational cost and moving objects are effectively modeled through the nonconforming technique.

In this work, the VEH model containing magnetic material in the coil is analyzed changing the geometric parameters. It is shown from the computational results that the VEH model with magnetic material in the coil has chaotic and linear oscillation modes. It is found that output power can be generated for a wide frequency range in the chaotic mode. Furthermore, in the linear mode, we can obtain large output power at the resonance.

Manuscript received June 26, 2013. Corresponding author: Takahiro Sato (e-mail: tsato@em-si.eng.hokudai.ac.jp).
Digital Object Identifier inserted by IEEE

II. Vibration Energy Harvesters

We consider a VEH device which consists of a coil and magnets fixed to the cantilever beam. The VEH device would be placed on the vibrating objects such as engines, motors, and bridges. The ambient vibration makes sinusoidal displacements of the magnets relative to the coil. As a result, the magnetic flux across the coil changes in time and consequently electromotive force (EMF) is induced. In addition, the current flowing in the coil generates weak magnetic force acting on the magnets. Because the weak magnetic force can be assumed as an electric damper, the vibrational behavior of the VEH devices can be modeled as the spring damper system [8], from which the output can be estimated. When the VEH device is assumed to have linearity, it has resonances. Relatively large output power can be obtained at the resonant frequencies.

In this paper, we analyze the VEH model shown in Fig. 1. The novelty in this device is that the magnetic material is introduced in the coil by which the flux path is designed to increase the flux across the coil. Simultaneously, the strong magnetic force acts on the magnets, owing to which it is expected that the cantilever has nonlinear oscillation.

When the VEH devices have complicated motion, the output cannot be evaluated from the simple spring damper model. For this reason, we introduce a coupled analysis

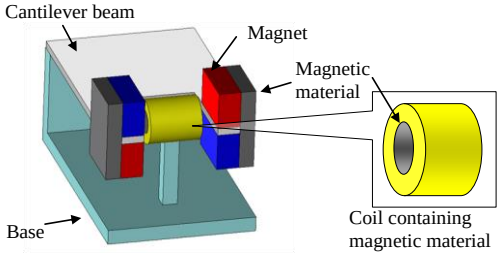

Fig. 1. Target vibration energy harvester model.

method for VEH, by which the behavior and output of any VEH devices can accurately be analyzed.

A. Coupled analysis method for vibration energy harvesters

Let us consider the governing equation of VEH. The cantilever motion is modeled as spring damper. The external circuit connected to the coil is represented by a resistive load for simplicity. Thus, the governing equations are given by

$$m\ddot{p} + c_{\mathrm{m}}(\dot{p} - \dot{q}) + k_{\mathrm{m}}(p - q) = F(\boldsymbol{A}), \tag{1}$$

$$\nabla \times \nu(\nabla \times \boldsymbol{A}) = \boldsymbol{J}_0 + \nu_0 \nabla \times \boldsymbol{M}, \tag{2}$$

$$\frac{\mathrm{D}\Phi}{\mathrm{D}t} + RI = 0, \tag{3}$$

where m is mass of objects on the tip of the cantilever, c_{m} and k_{m} are effective damping and stiffness coefficients of the cantilever, p is magnets position, and q is coil position which is equal to the input vibration, namely, $q=Q\sin(\omega t)$. In addition, $\boldsymbol{A}$, $\boldsymbol{M}$, ν and ν_0 are vector potential, magnetization vector, reluctivity of magnetic material and vacuum, respectively. Moreover, $F(\boldsymbol{A})$ and $\boldsymbol{J}_0$ are the magnetic force acting on the magnets and the current density, respectively, and R is the load resistance. The current I in (3) is obtained by integrating $\boldsymbol{J}_0$ on the cross-section of the electric circuit. In addition, D/Dt is Lagrange derivative to consider EMF due to the coil movement [11].

In the present method, the voxel-FEM is employed to solve (2). In this method, the nonconforming voxels for the device shapes are automatically generated with low computational cost [10]. This method is useful for designing new devices like VEH in which we must generate many FE meshes. Moreover, to treat the relative displacement between the coil and magnets, two voxel meshes are connected using the nonconforming technique [12] as shown in Fig. 2, in which mesh1 and mesh2 correspond to the coil and magnets, respectively. Nodal positions in mesh1 change corresponding to their relative displacement q-p. Then, unknowns along edges in mesh1 on the interface between two meshes are interpolated by those in mesh2. In the nonconforming technique, the unknowns assigned to the slave edges are expressed in terms of linear combination of the unknowns assigned to the master edges. Namely, the unknown, A_s, assigned to a slave edge, e_s, is interpolated by the master edges, A_i, as follows:

$$A_{\mathrm{s}} = \sum_{i=1}^{N_{\mathrm{mas}}} A_i \int_{e_s} \boldsymbol{N}_i \cdot d\boldsymbol{l} \equiv \sum_{i=1}^{N_{\mathrm{mas}}} c_{i,s} A_i, \tag{4}$$

where $\boldsymbol{N}_i$, $\boldsymbol{l}$, N_{mas} are the interpolation function of edge i, tangential vector along edge e_s, the number of the master edges, respectively, and $c_{i,s}$ represents the relation between the unknowns of edge i and s. The nonconforming edges in each voxel mesh are also interpolated in the similar way. Note that the master edges for a slave are easily found because edges are regularly placed in the voxel meshes. As a result of the interpolation, all the unknowns, $\boldsymbol{A}_{\mathrm{all}}$, can be expressed in terms of the unknowns along the master edges, $\boldsymbol{A}_{\mathrm{m}}$, in a form $\boldsymbol{A}_{\mathrm{all}}=\mathrm{C}\boldsymbol{A}_{\mathrm{m}}$, where C is $(N_{\mathrm{M}})\times(N_{\mathrm{M}}+N_{\mathrm{S}})$ matrix which expresses interpolation relations whose components consists of $c_{i,s}$, where N_{M} and N_{S} are the number of master and slave edges, respectively [10].

Here, the Lagrange coordinate system is employed to describe the motion of the mesh1. Hence, Lagrange derivative in (3) can simply be computed from

$$\frac{\mathrm{D}\Phi}{\mathrm{D}t} = \frac{1}{\Delta t}\boldsymbol{b}_u{}^{\mathrm{T}}\mathrm{C}(\boldsymbol{A}_n - \boldsymbol{A}_{n-1}), \tag{5}$$

where $(\boldsymbol{b}_u)_i=(\boldsymbol{j}_0, \boldsymbol{N}_i)$ is the dimensionless vector which contains the current density for unit current, $\boldsymbol{j}_0= \boldsymbol{J}_0/I$. In addition, $\boldsymbol{A}_n$, $\boldsymbol{A}_{n-1}$ are the variables defined in (4) whose dimension is Wb at time steps n, n-1, respectively.

The coupled analysis is performed using the staggered method [9]. Namely, (1), (2), and (3) are solved alternatively until convergence at each time step. This iteration is here called subcycle. In this work, (1) is solved by the Runge-Kutta method. The discretized governing equations are given by

$$\ddot{p}_n^k = -\frac{c_{\mathrm{m}}}{m}\left(\dot{p}_n^{k-1} - \dot{q}_n\right) - \frac{k_{\mathrm{m}}}{m}\left(p_n^{k-1} - q_n\right) + \frac{F\left(\boldsymbol{A}_n^{k-1}\right)}{m}, \tag{6}$$

$$\mathrm{C}^{\mathrm{T}}\mathrm{K}\mathrm{C}\boldsymbol{A}_n^k = \mathrm{C}^{\mathrm{T}}\boldsymbol{b}\left(I_n^{k-1}\right), \tag{7}$$

$$I_n^k = -\frac{1}{R\Delta t}\boldsymbol{b}(1)^{\mathrm{T}}\mathrm{C}\left(\boldsymbol{A}_n^{k-1} - \boldsymbol{A}_{n-1}\right), \tag{8}$$

where k is the step number in the subcycle, $\boldsymbol{b}(I)$ is right hand vector in FEM for I. When the all solutions converge in the subcycle, that is,

$$\left|p_n^k - p_n^{k-1}\right| < \varepsilon_p, \left\|\boldsymbol{A}_n^k - \boldsymbol{A}_n^{k-1}\right\| < \varepsilon_A, \left|I_n^k - I_n^{k-1}\right| < \varepsilon_I, \tag{9}$$

then n is incremented, and new subcycle starts. The flow of the coupled analysis is shown in Fig. 3.

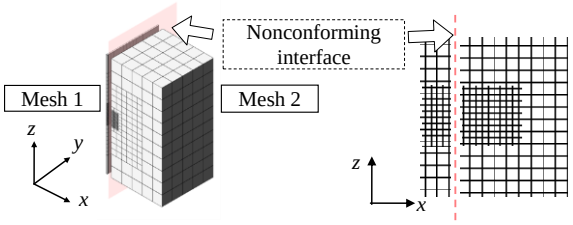

Fig. 2. Two nonconforming voxels for analysis of moving object.

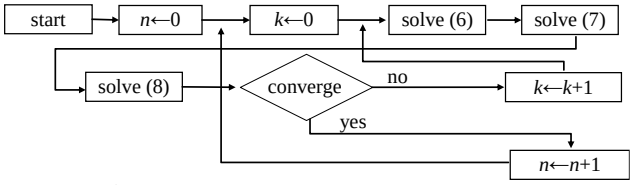

Fig. 3. Flow of coupled analysis method.

III. Simulations of VEH Model

A. Normalization

The VEH model shown in Fig. 1 is analyzed using the coupled analysis method. To consider the characteristic which is independent of dimension, the system is normalized. Here, length, time, weight and magnetic flux density are normalized by L_{T}, S_{T}, M_{T}, and B_{T}, respectively. Here, L_{T} and B_{T} are set to the gap between magnets, l_g, and the remanent flux density of Neodymium magnet, 1.2T, respectively. In addition, S_{T}, M_{T} are set to 0.05s, 1g, respectively. The normalized VEH model for the field analysis is shown in Fig. 4. After the normalization, equations (6)-(8) result in

$$\frac{\mathrm{d}^2\bar{p}_n^k}{\mathrm{d}\bar{t}^2}=\frac{1}{\bar{m}}\bar{F}\left(\bar{\boldsymbol{A}}_n^{k-1}\right)-\frac{\bar{c}_\mathrm{m}}{\bar{m}}\frac{\mathrm{d}}{\mathrm{d}\bar{t}}\left(\bar{p}_n^{k-1}-\bar{q}_n\right)-\frac{\bar{k}_\mathrm{m}}{\bar{m}}\left(\bar{p}_n^{k-1}-\bar{q}_n\right), \tag{10}$$

$$\mathrm{C}^\mathrm{T}\bar{\mathrm{K}}\mathrm{C}\bar{\boldsymbol{A}}_n^k=\mathrm{C}^\mathrm{T}\bar{\boldsymbol{b}}_n^{k-1}, \tag{11}$$

$$\bar{I}_n^k=-\frac{1}{\bar{R}\Delta\bar{t}}\bar{\boldsymbol{b}}_u{}^\mathrm{T}\mathrm{C}\left(\bar{\boldsymbol{A}}_n^{k-1}-\bar{\boldsymbol{A}}_{n-1}\right), \tag{12}$$

$$\bar{F}\left(\bar{\boldsymbol{A}}_n^k\right)\equiv S_\mathrm{T}{}^2F\left(L_\mathrm{T}B_\mathrm{T}\boldsymbol{A}_n^k\right)/L_\mathrm{T}M_\mathrm{T},\qquad \bar{m}\equiv m/M_\mathrm{T},$$
$$\bar{c}_\mathrm{m}\equiv S_\mathrm{T}c_\mathrm{m}/M_\mathrm{T},\qquad \bar{k}_\mathrm{m}\equiv S_\mathrm{T}{}^2k_\mathrm{m}/M_\mathrm{T}, \tag{13}$$

where overbar denotes normalized values, $\bar{F}\left(\bar{\boldsymbol{A}}\right)$ are normalized magnetic force, and $\bar{c}_\mathrm{m}$, $\bar{k}_\mathrm{m}$ are normalized damping, spring coefficients, respectively.

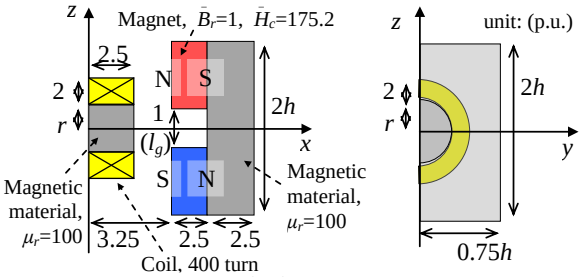

Fig. 4. Normalized VEH model for field analysis.

The behavior of this system highly depends on $\bar{F}\left(\bar{\boldsymbol{A}}\right)$ in (10). Therefore the coupled analysis is performed by changing the coil radius and magnets height, r and h. In this analysis, $\bar{c}_\mathrm{m}$, $\bar{k}_\mathrm{m}$, $\bar{R}$, and input amplitude are fixed to 1.0, 1125.0, 0.0011, and 0.25, respectively. In this work, nine conditions with different r and h summarized in Table I are considered in which the magnet size $\bar{m}$ is set to 1, 3, 5 when h is 5, 7.5 10, respectively.

B. Performance of voxel-FEM

We discuss here the performance of the present voxel-FEM. Fig. 5(a) shows the difference of computational results between the voxel-FEM and the conventional FEM with tetrahedral elements. The numbers of elements in former and later methods are 72,312 and 1,973,411, respectively. From Fig. 5(a), we can see that the maximum difference between two methods is less than 5%. Fig. 5(b) shows the computational time for mesh generation in the voxel-FEM. From Fig. 5(b) it can seen that the computational cost for mesh generation in the voxel-FEM is of order of n. Note that the computational cost for conventional tetrahedral mesh is of order of $n\log n$ [13]. From these results, we conclude that the voxel-FEM is suitable for computation of moving objects as well as optimization problems because of its high computational efficiency.

C. Numerical results

The coupled analysis is performed for nine cases shown in Table I. In these analyses, two input frequencies, f_1=1, f_2=4, are considered. Figure 6 shows the trajectories on the phase plane of the relative position $z=\bar{p}_n-\bar{q}_n$ and the relative velocity, v. Moreover, Fig. 7 shows the transitions of z and EMF, V, corresponding to the trajectories shown in Figs. 6(b) and 6(d). From these results, it can be seen that the behavior dramatically changes in dependence on r and h. In (A), chaotic nonlinear oscillations are observed at f_1 and f_2 as shown in Figs. 6(a) and 6(b). In (E), the cantilever has nonlinear oscillation at f_1, whereas it has linear oscillation at f_2. In these cases, the amplitude of z is relatively large for the computed frequency range. This suggests that output can be generated for the wide range of frequency through the nonlinear oscillation. On the other hand, in (D), the cantilever does not have oscillations at f_1, while linear oscillation is observed from f_2. This indicates that magnetic force does not give nonlinearity when r is relatively large.

It is found from the analysis results that the VEH model has chaotic and linear oscillation modes which vary by r and h. To show the complexity of the cantilever motion in each condition, the Lyapunov exponent, λ, for the nine conditions is computed using the Rosenstein's method [14]. Positive λ corresponds to chaotic oscillation, in contrast, negative λ corresponds to linear or limit cycle oscillation. Table II summarizes λ for the nine conditions at f_1 and f_2, where 0.0 means that the cantilever is not oscillated. From Table II, we can see that there is no oscillation in (B), (C), and (F) at f_1 while positive λ is obtained at f_2. In these conditions, the

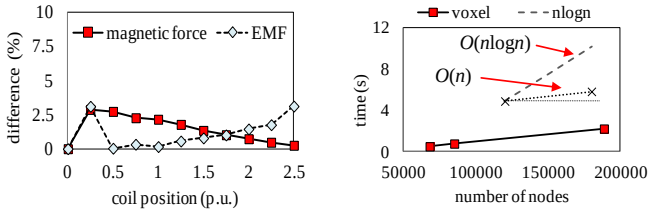

(a): computational accuracy (b): mesh generation time

Fig. 5. Performance of voxel-FEM.

TABLE I
ANALYSIS CONDITIONS

cond.	(A)	(B)	(C)	(D)	(E)	(F)	(G)	(H)	(I)
r	1.25	1.25	1.25	2.5	2.5	2.5	5	5	5
h	5	7.5	10	5	7.5	10	5	7.5	10

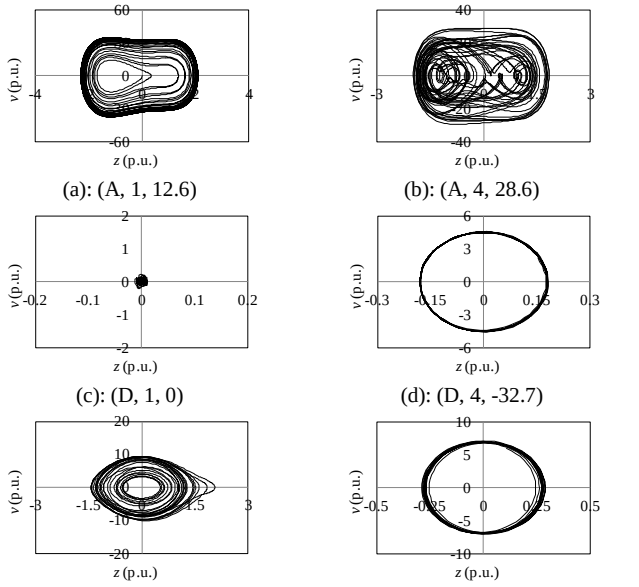

(a): (A, 1, 12.6) (b): (A, 4, 28.6)

(c): (D, 1, 0) (d): (D, 4, -32.7)

(e): (E, 1, 33.4) (f): (E, 4, -13.1)

Fig. 6. Trajectories for (cond., f, λ), where C_d, f, λ represents condition shown in Table I, normalized frequency, Lyapunov exponent, respectively.

magnet size is sufficiently large, as a result, the magnetic force is so strong that the relative position between the coil and magnets is fixed when the input frequency is relatively low. In (D), (G), (H), and (I), λ is negative at f_2, whereas the cantilever has no oscillation at f_1. These results suggest that the cantilever has linear oscillation when r/h is large. The reason why the cantilever is oscillated only at high frequency is that the resonant frequency for the fixed mechanical parameters is about 5. In (A) and (E), λ is positive and the cantilever can oscillate over the whole frequency range.

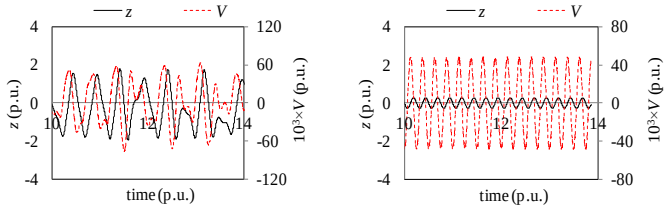

(a): (A, 4) (b): (E, 4)

Fig. 7. Transitions of z and V in conditions (cond., f).

TABLE II
LYAPUNOV EXPONENT FOR 9 CONDITIONS

	(A)	(B)	(C)	(D)	(E)	(F)	(G)	(H)	(I)
f_1	12.6	0.0	0.0	0.0	33.4	0.0	0.0	0.0	0.0
f_2	28.6	70.4	40.7	-32.7	-13.1	53.0	-67.9	-20.1	-18.2

D. *Output power against frequency*

The cantilever has relatively large oscillation amplitude at f_1 and f_2 in (A) and (E). This fact indicates that we can have wide frequency range for power generation in the chaotic mode. It is also shown that the cantilever has linear oscillation when r/h is large. In such case, it is expected that large output would be obtained at the resonance. To clarify the frequency characteristics, the output power against frequency is computed using the coupled analysis method for (A) and (D) is computed. Moreover, to reveal the effect on the magnetic material in the coil, the output of a VEH model without magnetic material in the coil when r and h are 2.25 and 5, respectively, is also computed. This condition is here called (L). In these analyses, the output is not normalized and l_g is set to 0.4mm.

The outputs against the input frequency for (A), (D), and (L) are shown in Fig. 8 where the output under 10μW is not plotted. It is clearly observed that output power over the whole range is larger than 0.1mW in (A). Hence, we can have wide bandwidth for power generation through the chaotic oscillation. It can be also seen from Fig. 8 that large output power is obtained in (D) when the input frequency is 120Hz. At the resonance, the output power in (D) is much grater than that of (L). This is due to the fact that the magnetic flux across the coil is effectively increased by the magnetic material.

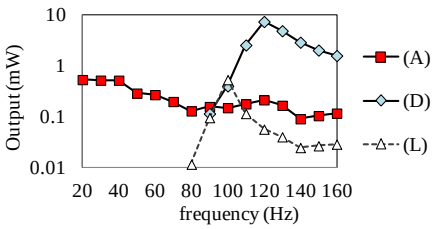

Fig. 8. Output power against frequency.

From these results, we conclude that the VEH device having chaotic oscillation is suitable for the operation in the environment where the ambient frequency is not predicted. In contrast, that having linear oscillation is effective when the input vibration is predictable.

IV. CONCLUSION

The coupled analysis method for VEH has been presented based on the voxel-FEM, by which the moving mechanical system can effectively be modeled without time-consuming mesh generations. Using the present method, the VEH model containing magnetic material in the coil has been analyzed. The analysis results show that the VEH device has chaotic oscillation which realizes wide frequency range for power generation. It is also shown that that has linear oscillation when the radius of the coil is large. In the linear oscillation, we have large output at the resonant frequency.

For the future works, the analysis results will be compared with measurement data.

ACKNOWLEDGMENT

This study was supported by research grants from Japan Power Academy and a Grant-in-Aid for Scientific Research (24310117).

REFERENCES

[1] S. P. Beeby, *et. al.*, "A micro electromagnetic generator for vibration energy harvesting," *J. Micromech. Microeng*. vol.17, pp. 1257-1265, 2007.

[2] D. Zhu, *et. al.*, "General model with experimental validation of electrical resonant frequency tuning of electromagnetic vibration energy harvesters," *Smart Mater. Struct*. vol.21, pp. 1-14, 2012.

[3] Y. Sang, *el. al.*, "A Vibration-Based Hybrid Energy Harvester for Wireless Sensor Systems," *IEEE Trans. Magn.*, vol.48, no. 11, pp.4495-4498, 2012.

[4] Y. Zhu, *et. al.*, "A Magnetoelectric Generator for Energy Harvesting From the Vibration of Magnetic Levitation,", *IEEE Trans. Magn.*, vol.48, no.11, pp. 3344-3347, 2012.

[5] T. Galchev, *et. al.*, "A Vibration Harvesting System for Bridge Health Monitoring Applications," *in PowerMEMS*, pp. 179-182, 2010.

[6] L. G. W. Tvedt, *et. al.*, "Nonlinear Behavior of an Electrostatic Energy Harvester Under Wide- and Narrowband Excitation," *Journal of Microelectromechanical systems*, vol.19, no.2, pp. 305-316, 2010.

[7] M. Ferrari, *et. al.*, "Improved energy harvesting from wideband vibrations by nonlinear piezoelectric converters," *Sensors and actuators A*, vol.162, pp. 425-431, 2010.

[8] N.G. Stephen, "On energy harvesting from ambient vibration," *Journal of Sound and Vibration*, vol.293, pp. 409–425, 2006.

[9] T. Niho, *et. al*., "Numerical Instability of Magnetic Damping Problem of Elastic Plate," *IEEE Trans. Magn.*, vol.36, no.4, pp. 1373-1376, 2000.

[10] T. Sato, *et. al.*, "3D Optimization of Ferrite Inductor Considering Hysteresis Loss," *IEEE Trans. Magn.*, vol.49, no.5, pp. 2129-2132, 2013.

[11] K. Muramatsu, *et. al.*, "Three-Dimensional Steady-State Eddy-Current Analysis of Moving Conductor Using Edge Elements and Moving-Coordinate System", *IEEE Trans. Magn.*, vol.38, no.2, pp. 597-600, 2002.

[12] H. Kometani, S. Sakabe, A. Kameari, "3-D analysis of induction motor with skewed slots using regular coupling mesh," *IEEE Trans. Magn.*, vol.36, no.4, pp. 1769-1773, 2000.

[13] S. W. Sloan, "A fast algorithm for constructing Delaunay triangulations in the plane", *Advances in Engineering Software*, vol.9, no.1, pp.34-55, 1987.

[14] M. Rosenstein, *et. al*., "A practical method for calculating largest Lyapunov exponents from small data sets," *Physica D*, vol.65, pp. 117-134, 1993.